Frascati Physics Series Vol. XXIV (2002), pp. 173-182
INTERNATIONAL SCHOOL OF SPACE SCIENCE - 2001 Course on
ASTROPARTICLE AND GAMMA-RAY PHYSICS IN SPACE, L'Aquila (Italy), 30/8 - 7/9, 2001

ANALYSIS OF COSMIC-RAY DATA: EXAMPLES WITH ANTIPROTONS AND POSITRONS

Mirko Boezio
Sezione INFN di Trieste, Via A. Valerio 2, I-34147 Trieste, Italy

ABSTRACT

Data analysis is a relevant part in the experimental-physics work. Here we will discuss it referring to the analysis of antiprotons and positrons in the cosmic radiation.

1 Introduction

Measurements of cosmic-ray antiparticles (antiprotons and positrons) are important for understanding several aspects of cosmic-ray physics. Their study permits to investigate the origin and propagation of cosmic rays in the Galaxy. Moreover, questions such as: do antimatter exist domains in the Universe? do mini-black holes exist and evaporates? is dark matter made up of supersimmetric particles? can be answered by these measurements.

To address these scientific topics a precise measurement of the antiproton and positron energy spectra in a wide energy range is needed. Fig. 1 shows the existing antiproton flux data. The experimental data are presented along

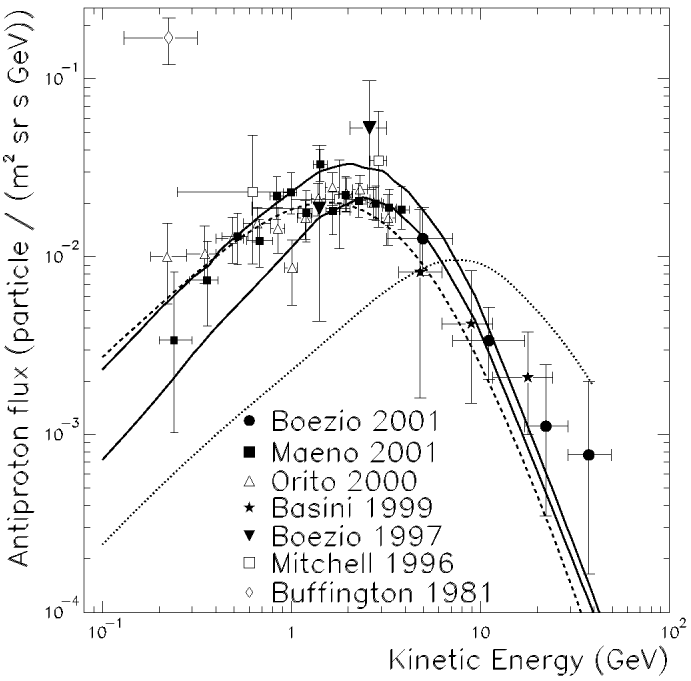

Figure 1: *The experimental* $\overline{\mathrm{p}}$ *spectrum* [1, 2, 3, 4, 5, 6, 7] *along with theoretical calculations* [8, 9, 10] *(see text).*

with different theoretical calculations which account for a pure secondary component [8, 9] (all antiprotons are produced by interaction of the cosmic-rays with the interstellar matter, solid and dashed lines) and for a primary component [10] (dotted line). The consistency among most of the experimental data is good and the measurements favour a pure secondary component. However, because of the limited statistics of these experiments, a primary component cannot be ruled out and the data are not precise enough to discriminate be-

tween different propagation models. In the following a brief description of the experimental and analysis procedure is provided.

2 Experimental measurements

Experimental study of primary cosmic rays requires that the measurements are performed outside the Earth's atmosphere or very close to the top of it so to minimize the atmospheric overburden. For this reasons, the experiments are attached to stratospheric balloons or on board of satellites. With the exception of the AMS experiment [11] on the space shuttle, all the existing measurements of antiparticles were obtained by balloon-borne experiments.

The difficulties of these measurements are mostly related to the fact that antiparticles are a rare component of the cosmic radiation. Antiprotons and positrons must be distinguished from a large background of protons and electrons. Furthermore, for balloon-borne experiments there is an additional background of products, such as muons and pions, of cosmic-ray interactions with the overlying atmosphere. Moreover, the data must be corrected for the secondary production in the atmosphere, which becomes increasingly important for energies below about a few GeV. The main goal of these experiments is to provide measurements of the fluxes of the cosmic-rays hence precise determination of the energy of the particle is required. In most experiments this was done using magnetic spectrometers with which the rigidity[1] of the particles was measured. While very precise, this technique, however, requires the study of the rigidity dependent background of spillover protons especially relevant for the antiproton analysis. In fact, due to the limited spectrometer resolution, high rigidity protons can mimic negative tracks and, hence, be tagged as antiprotons. Furthermore, reliable energy spectra measurements requires precise determination of the efficiencies of the various detectors.

Figure 2 shows CAPRICE98 apparatus [12], a balloon-borne experiment that gave results both on antiprotons and positrons, that illustrates some typical features of these type of cosmic-ray experiments. The CAPRICE98 apparatus, from top to bottom, consisted of: a gas Ring Imaging Cherenkov (RICH) detector [13], a time-of-flight (ToF) system, a magnet spectrometer and a silicon-tungsten imaging calorimeter [14]. The ToF system was used for

[1]Rigidity= momentum $\times$ speed of light/charge.

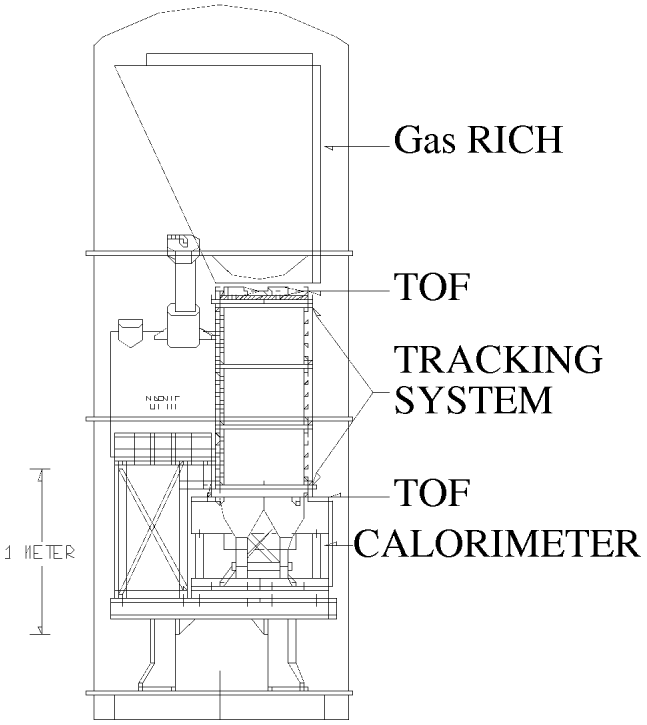

Figure 2: *The CAPRICE apparatus in the 1998 configuration (CAPRICE98).*

the trigger and to measure the time-of-flight and ionization losses of the particles. With this information single-charge down-going particles were selected rejecting helium and heavier nuclei, which are a consistent fraction of the cosmic radiation, and albedo particles, which are secondary particles produced in the atmosphere with an up-going direction. The magnet spectrometer had a superconducting magnet and a tracking device from which information the rigidity and charge sign of the particles were determined. The final selection of $\overline{\mathrm{p}}$ in a background of e^- , μ^- and π^- and of e^+ in a background of p, μ^+ and π^+ was performed with t the gas-RICH and the calorimeter. The RICH, for particles with velocity above its Lorentz threshold (about 19 for the C_4F_{10}

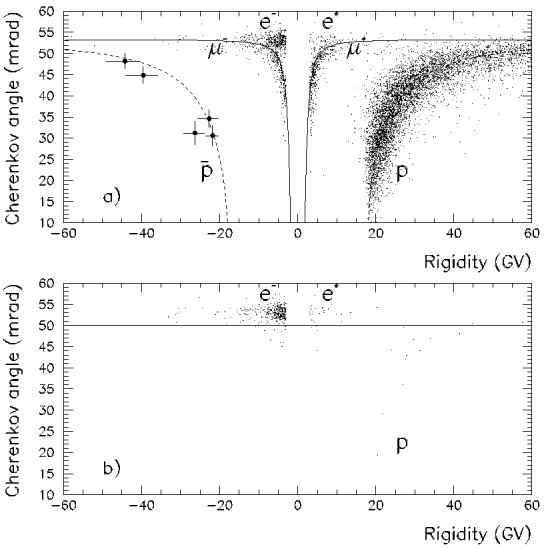

Figure 3: *The measured Cherenkov angle by the CAPRICE98 experiment as a function of rigidity. In a) the solid and dashed lines represent the theoretical values of the Cherenkov angle for muons and (anti)proton respectively. On the negative side, the location of five antiprotons are indicated with black squares together with one standard deviation errors on the measured rigidities and Cherenkov angles. In b) the events surviving the calorimeter electron selection are shown. The solid line indicates the lower limit for the RICH electron selection.*

gas), provided a measurements of their velocity through the reconstruction of the Cherenkov angle [13]. Comparing this information with the rigidity measured by the tracking system the particles can be identified. Fig. 3 shows the Cherenkov angle as measured by the RICH as a function of rigidity. Fig. 3 a) shows how the RICH information can be used to identify antiprotons: in correspondence of the antiproton band (dashed line) five antiprotons are clearly distinguishable from the e^- and μ^- background. Here they are shown with one standard deviation error bars for both the rigidity and Cherenkov angles measurements. Below the antiproton gas-RICH threshold (about 18 GV) an-

tiprotons can still be identified since no Cherenkov light is detected contrary to muons and electrons. This is valid down to the muon threshold, that is 2 GV. To extend the antiproton identification to lower energies a RICH detector can still be used replacing the gas with a radiator of higher refractive index. For example, a similar configuration of CAPRICE98 apparatus was flown in 1994, therefore called CAPRICE94, where sodium-fluoride (NaF, refractive index $\simeq 1.39$ and threshold Lorentz factor $\simeq 1.4$) was used as radiator and antiproton were identified between 0.6 and 3.2 GeV of kinetic energy [5].

It is clear from fig. 3 that the RICH can be used to identify positrons as well. However, in this case, the background of protons is so vast that additional information is needed for the separation. Furthermore, as can be seen in the figure, the RICH cannot separate μ^+ from e^+ above about 4 GV. The additional rejection is provided by the calorimeter. This calorimeter is a sampling calorimeter of 7 radiation lengths in which the electrons shower producing the typical electromagnetic cascades. Thanks to a fine longitudinal and transversal segmentation, along with the measurement of the energy losses in the sensitive elements (silicon layers), electromagnetic showers can be identified by imposing conditions on parameters describing their shape and energy distributions (for more information see [15]). The effect of the calorimeter selection can be seen in fig. 3 b) where only the events of fig. 3 a) passing the electron calorimeter selection are shown. Comparing the two figures it is evident that most of the contamination has been rejected and the electron and positron signals is easily extracted from the remaining background using the RICH information (i.e. selecting all the events above the solid line in figure).

Antiprotons and positrons have also been identified with other detectors. The BESS experiment [3] used a time-of-flight system providing high-resolution velocity measurements with which they selected antiprotons up to about 4 GV. The HEAT-pbar experiment [16] derived the particle velocity from multiple dE/dx measurements and measured antiprotons up to 50 GV. TS93 [17] and HEAT [18] experiments identified e^+ up to 50 GeV combing a transition radiation detector with an electromagnetic calorimeter.

3 Flux calculation

The flux is obtained from the relation

$$\text{Flux(E)} = \frac{1}{T_{live} \times G \times \Delta E \times TF} \times N^{TOA}(E),$$

where T_{live} is the total time during which the apparatus was able to record data, G is geometrical factor, ΔE the width of the energy interval[2] in which the events were selected and N^{TOA} the number of selected events scaled to the top of the atmosphere. T_{live} is usually obtained scaling the time of data taking by the dead time of the experiment. The geometrical factor accounts for the acceptance of the apparatus and the simplest way of calculating it is with Monte Carlo techniques [20]. ΔE is the energy bin corrected for ionization losses from the top of the atmosphere to the tracking system where the measurement is performed.

Using the information given by the various detectors described in the previous sections, $\overline{\text{p}}$ and e^+ are identified from the recorded data. In this process also the contamination by other particles is estimated and usually either subtracted from the selected sample or the rigidity interval, in which particles are selected, is chosen to have a negligible surviving contamination. Then, to obtained N^{TOA} , the numbers of particles selected in the spectrometer must be corrected for :

1. selection efficiencies;
2. losses of particles because of interaction with the detectors above the tracking system and the atmosphere overlying the apparatus and
3. secondaries produced in the atmosphere.

These corrections are rigidity dependent and have different effects in the flux estimation that are, often, quite significant. Efficiencies are usually estimated using either simulation or the flight data themselves. Both methods require a careful study of possible biases and variation in the performances of the detectors during the flight. For example, pressure changes, which normally happen during a balloon flight, for a gas-RICH as the CAPRICE98 RICH result

[2]Usually cosmic-ray fluxes are expressed in number of particles per (m^2 sr s GeV) and the energy is the kinetic energy.

in variation of the refractive index of the radiator and, consequently, of the Cherenkov threshold and number of Cherenkov photons produced. This clearly affects the performance of the detector and its selection efficiency. Overlooking these effects can results in significant errors on the fluxes. Sometime is not possible to precise determine these effects hence, the correct way to proceed is to estimate the uncertainty on the knowledge of these effects and propagate it as a systematic uncertainty in the flux calculation.

Atmospheric secondaries are obtained from calculations and they represent a significant component of the measured antiprotons and positrons. For example fig. 4 shows the e^- and e^+ spectra measured by the CAPRICE94 experiment [15] at 3.9 g/cm^2 of residual atmosphere. The solid and dashed lines shows the estimated contributions of atmospheric e^- and e^+ , respectively. The data were taken at a vertical geomagnetic cutoff of about 0.5 GV. It can be seen that, except below 1 GeV, the secondary electron component accounts for a few percent of the primary component, hence, assuming that all electrons are of primary origin would result in a small error. However, this does not hold for positrons: for all energies the secondary component is an important fraction of the positron flux and the data must be corrected for it. This also means that uncertainties on the secondary calculation will reflect significantly on the flux estimations.

4 Conclusions

Measurements of cosmic rays are very challenging because of the environmental difficulties in which these experiments take place. This, consequently, affects the data analysis and it is even more true for antiparticle searches because of the paucity of these particles in the cosmic radiation. Therefore, along with the study of the detector outputs to derive good selection conditions and to estimated the background contamination a careful analysis of all assumptions made for estimating the final result has to be performed. From these analysis statistical and systematic errors are derived and they have to be included in the final result. For example, the data in fig. 1 include both statistical and systematic uncertainties. However, it is worth pointing out that an additional systematic uncertainty is not clearly indicated in this figure and often overlooked: the uncertainty on the energy (rigidity) determination. This quantity is often not very well known since it requires an independent energy measure-

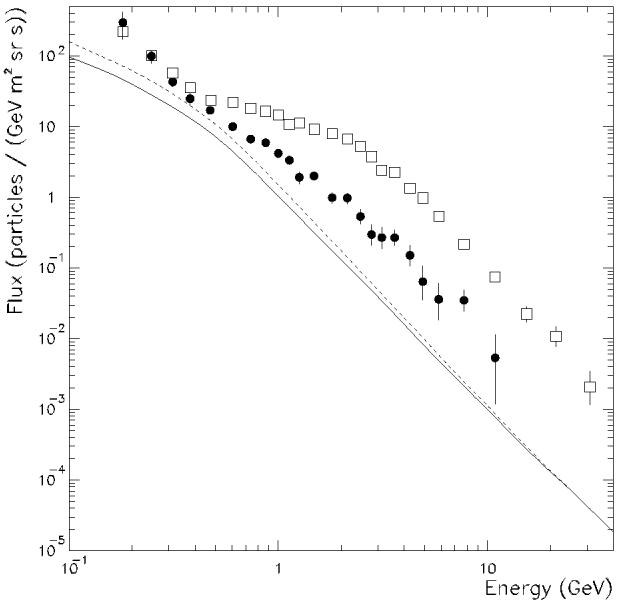

Figure 4: *The electron (□) and positron (•) spectra measured at top of the payload by the CAPRICE94 experiment* [19] *and the calculated atmospheric electrons (solid line) and positrons (dashed line) at 3.9 g/cm² of residual atmosphere* [21].

ment that is often not available during the experiment. Also calibration at a test beam facility at ground prior or after the flight is often not sufficient to represent the experimental conditions since the devices can suffer variation and misalignments during the launch phase.

References

1. M. Boezio *et al.*, astro-ph/0103513 (2001).
2. T. Maeno *et al.*, Astropart. Phys. **16**, 121 (2001).
3. S. Orito *et al.*, Phys. Rev. Lett. **84**, 1078 (2000).

4. G. Basini *et al.*, in Proc. 26th Int. Cosmic-Ray Conf., **4**, 77 (The University of Utah, Salt Lake City, 1999); see also M. Hof *et al.*, Astrophys. J. **467**, L33 (1996).

5. M. Boezio *et al.*, Astrophys. J. **487**, 415 (1997).

6. J. Mitchell *et al.*, Phys. Rev. Lett. **76**, 3057 (1996)

7. A. Buffington, S. M. Schindler and C. R. Pennypacker, Astrophys. J. **248**, 1179 (1981).

8. M. Simon, A. Molnar and S. Roesler, Astrophys. J. **499**, 250 (1998).

9. L. Bergström, J. Edsjö and P. Ullio, Astrophys. J. **526**, 215 (1999) and L. Bergström and P. Ullio, private comunication (1999).

10. P. Ullio, astro-ph/9904086 (1999).

11. J. Alcaraz *et al.*, Phys. Lett. B **484**, 10 (2000).

12. M. L. Ambriola *et al.*, Nucl. Phys. (Proc. Suppl.) B **78**, 32 (1999).

13. D. Bergström et al., Nucl. Instr. and Meth. **A 463**, (2001) 161.

14. M. Bocciolini et al., Nucl. Instr. and Meth. **A370**, (1996) 403.

15. M. Boezio *et al.*, Astrophys. J. **532**, 653 (2000).

16. A. S. Beach *et al.* astro-ph/0111094.

17. R. L. Golden *et al.*, Astrophys. J. **457**, L103 (1994).

18. S. W. Barwick *et al.*, Astrophys. J. **498**, 779 (1998).

19. M. Boezio1, Ph.D. thesis, Royal Institute of Technology, Stockholm, Sweden (1998).

20. J. D. Sullivan, Nucl. Instr. and Meth. **95**, (1971) 5.

21. A. S. Stephens, in Proc. 17th Int. Cosmic-Ray Conf., **4**, 282 (Commissariat a l'Energie Atomique, Gif-sur-Yvette, Essonne, France, 1981)